PAPER

Monolithic metal–organic frameworks for carbon dioxide separation†

David G. Madden, [ID] ‡[a] Robin Babu,‡[a] Ceren Çamur, [ID] [a] Nakul Rampal, [ID] [a] Joaquin Silvestre-Albero, [ID] [b] Teresa Curtin [ID] [c] and David Fairen-Jimenez [ID] *[a]

Carbon dioxide (CO_2) is both a primary contributor to global warming and a major industrial impurity. Traditional approaches to carbon capture involve corrosive and energy-intensive processes such as liquid amine absorption. Although adsorptive separation has long been a promising alternative to traditional processes, up to this point there has been a lack of appropriate adsorbents capable of capturing CO_2 whilst maintaining low regeneration energies. In the context of CO_2 capture, metal–organic frameworks (MOFs) have gained much attention in the past two decades as potential materials. Their tuneable nature allows for precise control over the pore size and chemistry, which allows for the tailoring of their properties for the selective adsorption of CO_2. While many candidate materials exist, the amount of research into material shaping for use in industrial processes has been limited. Traditional shaping strategies such as pelletisation involve the use of binders and/or mechanical processes, which can have a detrimental impact on the adsorption properties of the resulting materials or can result in low-density structures with low volumetric adsorption capacities. Herein, we demonstrate the use of a series of monolithic MOFs ($_{mono}$UiO-66, $_{mono}$UiO-66-NH$_2$ & $_{mono}$HKUST-1) for use in gas separation processes.

Introduction

Anthropogenic emissions of carbon dioxide (CO_2) are acknowledged to be a significant risk to the global climate. The atmospheric CO_2 concentration has surpassed 400 ppm on several occasions since 2013, which represents an increase

[a]Adsorption & Advanced Materials Laboratory (A²ML), Department of Chemical Engineering & Biotechnology, University of Cambridge, Philippa Fawcett Drive, Cambridge, CB3 0AS, UK. E-mail: df334@cam.ac.uk

[b]Laboratorio de Materiales Avanzados, Departamento de Química Inorgánica, Universidad de Alicante, San Vicente del Raspeig, E-03690, Spain

[c]Bernal Institute, Department of Chemical Sciences, University of Limerick, Limerick, V94 T9PX, Republic of Ireland

† Electronic supplementary information (ESI) available. See DOI: 10.1039/d1fd00017a

‡ These authors contributed equally.
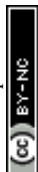
of over 100 ppm compared to pre-industrial revolution levels.[1] Carbon capture will be a crucial technology in achieving carbon neutrality by 2050.[2] While clean technologies such as wind and solar power will play a major role in energy provision over the coming decades, increasing energy demands dictate that fossil fuels will remain a key component of the global energy system into the second half of this century.[3] Additionally, CO_2 represents a significant impurity in industrial processes and its removal from important gases such as methane (CH_4) can help improve the overall quality of pipeline grade natural gas (NG). The upgrading of alternative forms of CH_4 such as biogas and landfill gas to produce biomethane is also an incredibly attractive source of renewable NG that, once purified, can be pumped directly into the national grid. The development of next-generation carbon capture and sequestration (CCS) technologies in the coming decades will be imperative in the fight again global climate change.

To date, CCS has been hampered by high costs (>100 US$ per t CO_2 captured) and the techno-economic uncertainties of liquid amine-based technologies.[4] Liquid amine-based CCS technologies have been around for over half a century. However, liquid amine chemical capture relies upon chemical reactions and is energy intensive, therefore reducing the overall efficiency of a power plant by up to 40%.[5] Additionally, liquid amines are volatile and prone to foaming, leading to the corrosion of industrial equipment. Liquid amines are thus not economically viable and offer little room for innovation. With the advent of the 2015 Paris agreement,[6] there has been a political shift towards reducing CO_2 emissions globally. In particular, Canada recently announced a direct tax on carbon emissions of at least 10 C$ per t, rising by 10 C$ per t per year until it reaches 50 C$ per t by 2022.[7] At 50 C$ per t, this will significantly improve the competitiveness of CCS technologies. Similar ambitious CO_2 emission reduction targets have been set in Europe and, right now, a new approach to CCS technologies is required, since renewable and new energy technologies alone will be unable to sustain the growing demand for energy in Europe. This requires a new paradigm for CCS technologies that will fundamentally improve the environmental footprint and cost effectiveness of CSS technologies.

As an alternative to traditional amine-based technologies, solid adsorbents represent a viable alternative for the next generation of low-temperature CCS technologies. To date, much of the research into solid adsorbent based CO_2 capture has focused on traditional porous materials such as zeolites, activated carbons and amine-modified silicas.[7–11] While significant progress has been made, there are many drawbacks to these materials. In the case of zeolites and activated carbons, these materials lack the tunability and chemical functionalities to improve important process parameters such as chemical interactions, selectivity and hydrophobicity, leading to high CO_2 capture costs as a result of their low working capacities and high regeneration costs. Similarly, amine-modified adsorbents rely on similar capture mechanisms to liquid amines and require elevated temperatures (>100 °C) for adsorbent regeneration. Besides, gas constituents such as NO_x, SO_x and CO_2 itself can negatively impact amine-modified solids by poisoning the chemisorbent and deactivating the amine adsorption sites.[12–14] Furthermore, amine-modified materials are sometimes subject to thermal and oxidative degradation.[15,16]

As an alternative to traditional porous materials, metal–organic frameworks (MOFs)[17,18] or porous coordination polymers (PCPs)[19] represent a broad class of

materials that have received a great deal of attention over the past two decades. MOFs are composed of metal ions or clusters, commonly referred to as nodes, bridged by organic ligands and in some cases organic and inorganic pillars, to form various structures and networks. There are currently *ca.* 100 000 MOF[20,21] structures included in the Cambridge Structural Database – MOF subset *vs. ca.* 1000 silicas and zeolites; their tuneable nature enables the precise control of the material design at the molecular level. Using crystal engineering and reticular chemistry approaches, it is possible to tailor the pore size and chemistry by the rational selection of the organic ligand, functional group, metal ion and activation method. MOFs have already displayed exceptional performance for a wide array of applications including gas storage,[22–24] catalysis[25,26] and drug delivery.[27–30] Their performance for gas separation has also been widely studied, with MOFs having benchmark physisorptive performances for numerous processes including carbon capture,[9] CO_2 direct air capture (DAC),[31–33] C2/C3/C4 separation[34–36] and natural gas processing.[37–39] The tunability of MOFs and the vast array of platforms available gives MOFs great promise for revolutionising industrial processes in the coming decades.

Despite their potential, the lack of a suitable method for production scale-up and shaping has thus far been a barrier to maximising the potential of MOFs for numerous applications. Their synthesis traditionally relies on solution-based methods, *i.e.* layering or solvothermal synthesis, both of which are time-consuming and require large amounts of solvent. Mechanochemical synthesis has recently garnered attention for adsorbent scale-up,[22–29] where the synthesis can be conducted at scale using continuous processes such as twin-screw extrusion (TSE).[30–36] While the scale-up of MOFs has been well-studied, these processes generally lead to powdered materials that require post-synthetic shaping. Indeed, the shaping of MOF powders into bulk samples with desired sizes, shapes, densities and mechanical stabilities is a critical step for their industrial deployment, as it is required to minimise pressure drops and to increase the volumetric adsorption capacity in adsorption columns (Fig. 1).[22] To date, mechanical shaping
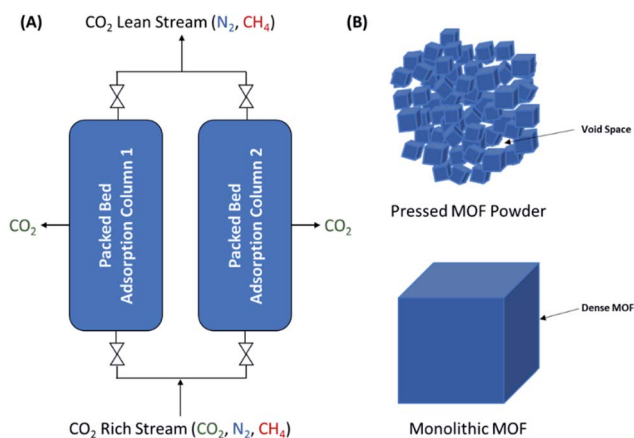

Fig. 1 (A) Schematic of a dual-column pressure swing adsorption/temperature swing adsorption (PSA/TSA) system with MOF packed beds. (B) Representation of the abundant void spaces amongst pressed MOF particles compared with a densified monolithic MOF.

using binders has already been widely utilised for shaping MOFs.[33,38–43] While mechanical shaping is relatively simple and fast, the resulting materials often display two major issues. On one hand, extruded materials where low mechanical pressures are applied display low bulk densities due to the presence of large void spaces. Conversely, in powder pressing, the delicate crystalline structures of MOFs are prone to collapsing under high mechanical pressures, leading to crumple zones of amorphous material.[20] These amorphous phases can give way to pellets with high bulk densities but with large reductions in the overall porosity. The development of strategies that can address the issues of powder processing whilst maintaining the gas separation performance is critical for the real-world applications of solid adsorbents.

In contrast to traditional shaping, self-shaping methods can effectively circumvent the issues related to the extrusion and high-pressure pressing of MOFs. Self-shaping can eliminate the need for additives and/or the use of mechanical presses or extruders. These unique methodologies hold promise for reducing the performance-related issues of MOF shaping whilst simultaneously reducing the cost for shaped MOF production. So far, there have been a limited number of reports on self-shaping MOFs.[44–52] In early self-shaping MOFs, researchers utilised precursor MOF gels to form self-shaped materials *via* syneresis when the MOF gel was dried under ambient conditions, while elevated drying temperatures gave way to powder formation.[53–56] These materials displayed similar properties to xerogels, displaying large volumes of hierarchical porosity and low bulk densities. The development of MOF xerogels gave way to the development of the first monolithic MOFs ($_{mono}$MOFs). Similar to previously reported monolithic gels, $_{mono}$MOFs have been formed *via* a sol–gel synthesis approach which has offered a viable alternative to traditional MOF shaping processes. $_{mono}$MOFs enable the synthesis of high-density, mechanically and chemically stable, centimeter-scale shaped materials, which retain their porosity during synthesis. The first such report on $_{mono}$MOF synthesis came with the development of $_{mono}$ZIF-8.[60] The transparent, glassy-looking material displayed a high BET area ($S_{BET} = 1423$ m^2 g^{-1}) and a density of $\rho_b = 1.05$ g cm^{-3} (single crystal $\rho_b = 0.95$ g cm^{-3}).

The sol–gel synthesis approach in MOFs was subsequently extended to other classical MOFs such as HKUST-1 and UiO-66.[49,50] The remarkable physical properties displayed by $_{mono}$HKUST-1 ($\rho_b = 1.06$ g cm^{-3} and $S_{BET} = 1288$ m^2 g^{-1}) resulted in an outstanding volumetric methane uptake capacity of 261 cm^3 (STP) cm^{-3} (65 bar, 298 K). This was found to substantially exceed the previously reported results for pelletised HKUST-1 compacted under a range of pressures and effectively rendered it as the first material to reach the DOE target for NG storage.[61] Recently, the formation of $_{mono}$UiO-66 was achieved by varying the sol–gel drying conditions employed during synthesis.[49] The bulk physical properties of $_{mono}$UiO-66 were tuned with a high level of experimental control, resulting in materials with bulk densities varying between 0.43 and 1.05 g cm^{-3} (single crystal $\rho_b = 1.20$ g cm^{-3}). The inclusion of mesoporosity and its resultant alteration of the adsorptive properties of the MOF yielded outstanding improvements in the methane working capacity of $_{mono}$UiO-66 (261 cm^3 (STP) cm^{-3}, 5–100 bar, 298 K). This demonstrated that unprecedented levels of synthetic control can be exerted on local structures of $_{mono}$MOFs, enabling the enhancement of the gas adsorption properties beyond those of purely microporous materials. While the field of
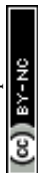
mono MOFs is relatively new, these materials have shown potential as viable alternatives to traditional shaping methods to produce high-density materials for industrial use.

In this contribution, we examine the gas separation performance of monoMOFs in comparison to their powdered variants under both gravimetric and volumetric conditions. The performances of all of the materials were then evaluated using single-component isotherms, gravimetric gas uptake and mixed gas dynamic breakthrough experiments. We used single-component isotherms to determine important parameters such as the gas uptake and mixed gas selectivity values, while we used gravimetric uptake experiments to determine the gas uptake kinetics. Finally, we analysed these materials for mixed gas separation in gas streams associated with carbon capture (15/85 v/v CO_2/N_2, dry and 74% relative humidity) and natural gas/biogas upgrading (50/50 v/v CO_2/CH_4). This work represents the first demonstration of the use of monoMOFs for gas separation applications.

Results & discussion

Synthesis, characterisation and physicochemical properties

Monolithic and powdered variants of HKUST-1, UiO-66 and UiO-66-NH$_2$ were initially synthesised *via* previously reported methodologies.[57–59,62–64] The crystallinities and thermal stabilities of the pristine samples were investigated using powder X-ray diffraction (PXRD) and thermogravimetric analysis (TGA), respectively. The experimental PXRD patterns were found to match the calculated PXRD patterns for each material. The PXRD patterns for the monolithic samples display Scherrer line broadening, caused by the non-convergence of the diffraction line in nano-size particles (Fig. S1–S3†). Besides, monolithic HKUST-1, UiO-66 and UiO-66-NH$_2$ were found to be thermally stable up to 300 °C, 400 °C and 280 °C, respectively (Fig. S4†), which is consistent with previous reports for these materials.
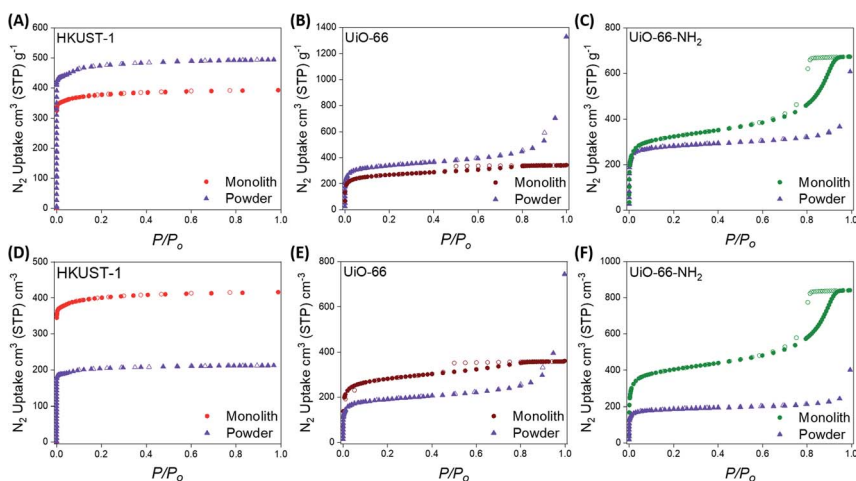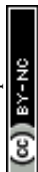

Fig. 2 Gravimetric (A–C) and volumetric (D–F) N$_2$ adsorption isotherms at 77 K for the monolithic and powdered HKUST-1, UiO-66 and UiO-66-NH$_2$ materials. Closed symbols represent adsorption while open symbols represent desorption.

Table 1 Textural and adsorption properties of the monolithic and powdered MOF samples. BET area (S_{BET}), total pore volume (V_{Tot}), bulk density (ρ_{bulk}) and gravimetric and volumetric CO_2 uptake measured for monolithic, pelletised and powdered HKUST-1, UiO-66 and UiO-66-NH$_2$ single component adsorption isotherms and dynamic mixed gas breakthrough studies

Materials	S_{BET} m² g⁻¹	V_{Tot}^{a} cm³ g⁻¹	ρ_{bulk}^{b} g cm⁻³	$\rho_{crystal}$ g cm⁻³	S_{BET} m² cm⁻¹	V_{Tot} cm³ cm⁻³	Single component gas adsorption				Dynamic breakthrough studies	
							CO_2 uptake (0.15 bar) cm³ g⁻¹ (cm³ cm⁻³)	CO_2 uptake (0.5 bar) cm³ g⁻¹ (cm³ cm⁻³)	S_{CN}^{c} (0.15 bar)	S_{CM} (0.5 bar)	CO_2 uptake 15/85 CO_2/N_2 cm³ g⁻¹ (cm³ cm⁻³)	CO_2 uptake 50/50 CO_2/CH_4 cm³ g⁻¹ (cm³ cm⁻³)
mono HKUST-1	1512	0.634	1.060	0.883	1603	0.672	18.5 (19.6)	53.8 (57.0)	23	12	21.3 (22.6)	53.3 (56.5)
powd HKUST-1	1871	1.290	0.500	0.883	936	0.645	23.8 (11.9)	76.2 (38.1)	—	—	24.7 (12.4)	61.7 (30.8)
pell HKUST-1^{c}	1340	0.570	0.824	0.883	1102	0.470	—	—	—	—	—	—
mono UiO-66	1015	0.530	1.050	1.237	1066	0.557	14.9 (15.6)	33.1 (34.8)	28	36	15.2 (16.0)	42.0 (44.1)
powd UiO-66	1288	2.050	0.560	1.237	721	1.148	18.1 (10.1)	39.9 (22.3)	—	—	17.9 (10.0)	44.0 (24.6)
pell UiO-66^{d}	1459	0.540	0.430	1.237	627	0.232	—	—	—	—	—	—
mono UiO-66-NH$_2$	1226	1.040	1.250	1.246	1533	1.300	15.1 (18.9)	34.9 (43.6)	30	54	16.0 (20.0)	36.2 (45.2)
powd UiO-66-NH$_2$	1094	0.941	0.660	1.246	722	0.621	17.2 (11.4)	39.7 (26.2)	—	—	17.6 (11.6)	38.5 (25.5)
pell UiO-66-NH$_2^{d}$	625	0.250	0.930	1.246	581	0.234	—	—	—	—	—	—

^{a} Obtained at P/P_o = 0.98. ^{b} Quantified using Hg porosimetry. ^{c} Quantified using ideal adsorption solution theory (IAST).[66] Physical properties for pellUiO-66 and pellUiO-66-NH$_2$ obtained from the study by Dhainaut et al.[68] ^{d} Physical properties for pellHKUST-1 obtained from the study by Peng et al.[67]

Further characterisation of the synthesised materials was performed using 77 K N_2 adsorption isotherms (Fig. 2) and Hg porosimetry (Table 1) to analyse the porosity and bulk densities, respectively, of the powdered and monolithic materials. Table 1 displays the BET areas (S_{BET}) calculated using our extended Rouquerol's criteria using our BETSI protocol (Fig. S8–S13†),[65] as well as the total (V_{tot}) pore volumes and bulk densities (ρ_{bulk}) of each material synthesised. All of the materials were fully activated by heating under vacuum before performing the porosimetry experiments. The experimental BET areas calculated for the powdered materials were consistent with those previously reported for HKUST-1, UiO-66 and UiO-66-NH_2.[62–64] The BET areas of the $_{mono}$MOFs were also consistent with previous reports.[57,58] For both the powdered and monolithic variants, the N_2 isotherms displayed high gas uptake below 0.1 P/P_o, indicating extensive microporosity within the samples. N_2 uptake was also observed at higher relative pressures (>0.8 P/P_o) for the Zr-MOFs, indicating the presence of mesoporosity. $_{mono}$UiO-66-NH_2 displayed a relatively large mesoporous step, while the lower N_2 uptake above 0.8 P/P_o for $_{mono}$UiO-66 indicates a relatively low amount of mesoporosity. This mesoporosity has been previously observed for $_{mono}$Zr-MOFs and can be attributed to the void spaces between the crystallites and UiO-type material defects.[57]

To investigate the bulk density properties of the synthesised materials, we performed Hg porosimetry on the monolithic and powdered MOF materials (Table 1). We have shown previously that $_{mono}$MOFs display higher bulk densities than powders and pelletised materials due to the exceptional control and close packing of the primary particles (*i.e.* crystallites) during the sol–gel synthesis. In turn, this leads to materials that maintain their porosity and performances and overcomes the limitations of traditional shaping techniques (*i.e.* pore collapse or low density due to high or low pressure, respectively, during the compression or pore blockage due to the use of binders). The bulk densities observed for $_{mono}$HKUST-1 (ρ_{bulk} = 1.06 g cm^{-3}), $_{mono}$UiO-66 (ρ_{bulk} = 1.05 g cm^{-3}), and $_{mono}$UiO-66-NH_2 (ρ_{bulk} = 1.25 g cm^{-3}) were comparable to previous reports.[57,58] In contrast, the bulk densities of the powdered materials were significantly lower for HKUST-1 (ρ_{bulk} = 0.5 g cm^{-3}), UiO-66 (ρ_{bulk} = 0.56 g cm^{-3}) and UiO-66-NH_2 (ρ_{bulk} = 0.66 g cm^{-3}). The lower density can be attributed to the poor packing, leading to large amounts of void space in the powder samples. When the bulk density is taken into account to calculate the volumetric BET area and volumetric total pore volume of each material (Table 1), the monolithic materials display significantly higher values compared to the powdered variants. In terms of performance, the monolithic materials display volumetric BET areas which are 79%, 48% and 150% higher for HKUST-1, UiO-66 and UiO-66-NH_2, respectively, compared to their powdered variants.

Single-component gas adsorption isotherms and kinetic studies

The exceptional physical properties of the $_{mono}$MOFs prompted us to examine their CO_2 adsorption and separation performances. We collected CO_2, N_2 and CH_4 single-component isotherms at 298 and 273 K for all monolithic materials (Fig. 3 & S14–S16†). We also collected CO_2 single-component isotherms at 298 K for the powdered variants for comparison (Fig. 3 & S17–S19†). The CO_2 uptake values at 298 K and 1 bar observed for $_{mono}$HKUST-1, $_{mono}$UiO-66 and $_{mono}$UiO-66-NH_2 were found to be 4.2, 2.2 and 2.1 mmol g^{-1}, respectively. The CO_2 uptake values for the
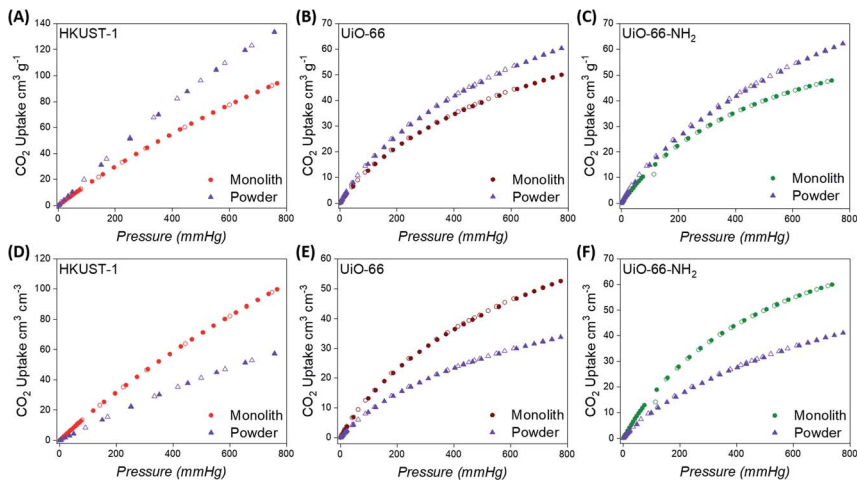
Fig. 3 Gravimetric (A–C) and volumetric (D–F) CO_2 adsorption isotherms at 298 K for monolithic and powdered HKUST-1, UiO-66 and UiO-66-NH$_2$ materials. Closed symbols represent adsorption while open symbols represent desorption.

monolithic MOFs were found to be consistent with values reported for the powdered variants of each material in the literature and in the NIST/ARPA-E Database of Novel and Emerging Adsorbent Materials.[9,69,70] Similarly, the lower uptake values for N_2 and CH_4 gases observed for the monoliths were also consistent with previous reports for powdered variants of each MOF material.[9,69,70] Although the powdered materials display higher gravimetric CO_2 adsorption performances compared to the monolithic materials for each MOF variant, this trend is once again reversed when the bulk density is used to calculate the volumetric CO_2 adsorption performance (Fig. 3). In this case, the monolithic variants display a superior volumetric performance. While many studies report the gravimetric CO_2 uptake performances of MOF materials, the volumetric performances of MOFs are often reported based on the crystal densities of the MOFs as opposed to the experimental bulk densities. To the best of our knowledge, the volumetric CO_2 uptake value for $_{mono}$HKUST-1 of 99.7 cm^3 cm^{-3} at 1 bar represents a new benchmark for volumetric performance under these conditions for MOF materials.

To examine the effect of MOF shaping on the adsorbent–adsorbate interactions, we collected variable temperature gas adsorption isotherms to determine the CO_2 isosteric heats of adsorption (Q_{st}) for the $_{mono}$MOF materials. To obtain the CO_2 adsorption energies for these compounds, we fitted the CO_2 adsorption data at 273 and 298 K using the virial equation (Fig. S20–S22†), calculating the Q_{st} using the Clausius–Clapeyron equation (Fig. S23†). $_{mono}$HKUST-1 displays a CO_2 Q_{st} of ca. 25 kJ mol^{-1}, while $_{mono}$UiO-66 and $_{mono}$UiO-66-NH$_2$ display values of ca. 25 and 37 kJ mol^{-1}, respectively, similar to previous reports for the powdered variants of each MOF material.[69,70] The higher Q_{st} displayed by $_{mono}$UiO-66-NH$_2$ can be attributed to the higher electrostatic contribution of the amino group which, in turn, leads to stronger adsorbent–adsorbate interactions.

To estimate the CO_2/N_2 (S_{CN}) and CO_2/CH_4 (S_{CM}) selectivities of the materials, we first fitted the adsorption isotherms to a dual-site Langmuir–Freundlich

This journal is © The Royal Society of Chemistry 2021
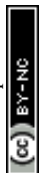
(DSLF) model (Tables S1–S3†) and then we used the ideal adsorbed solution theory (IAST).[66] We estimated the selectivities under the relevant conditions for carbon capture and natural gas purification (CO_2 mole fractions of 0.15 and 0.5, respectively) for all monolithic MOF materials (Fig. S24–S26†). For the CO_2 separations associated with carbon capture, $_{mono}$HKUST-1, $_{mono}$UiO-66 and $_{mono}$UiO-66-NH$_2$ exhibited IAST S_{CN} values (at 1 bar and 298 K) of 23, 28 and 30, respectively. For the CO_2 separations associated with natural gas purification, $_{mono}$HKUST-1, $_{mono}$UiO-66 and $_{mono}$UiO-66-NH$_2$ exhibited IAST S_{CM} values (at 1 bar and 298 K) of 12, 36 and 54, respectively. The high S_{CN} and S_{CM} values exhibited by the monolithic MOFs suggest that they have potential for use in gas separations relevant to post combustion carbon capture (15/85 v/v CO_2/N_2) and natural gas purification (50/50 v/v CO_2/CH_4).

We examined further the CO_2 adsorption performances of the monolithic materials using kinetic studies on pristine samples of $_{mono}$HKUST-1, $_{mono}$UiO-66 and $_{mono}$UiO-66-NH$_2$ (Fig. S30–S32†). We exposed the activated samples of the monolithic MOFs to a constant 20 ml min^{-1} flow of 1.0 bar CO_2 at 308 K, while constantly recording the weight change. We found that, despite having shaped the MOFs into larger bodies than the microcrystalline powder, the CO_2 uptake kinetics were consistent with previous reports,[32,33] with $_{mono}$HKUST-1, $_{mono}$UiO-66 and $_{mono}$UiO-66-NH$_2$ achieving 90% saturation loading in 60, 80 and 40 min, respectively. This demonstrates negligible loss in terms of the gas adsorption kinetics between the powdered and monolithic materials, something that is critical when evaluating the utility of monolithic materials for use in gas separation applications.

Dynamic mixed gas breakthrough studies

At this point, we examined the gas separation performances of the $_{mono}$MOFs using experimental breakthrough studies on the pristine samples of powdered
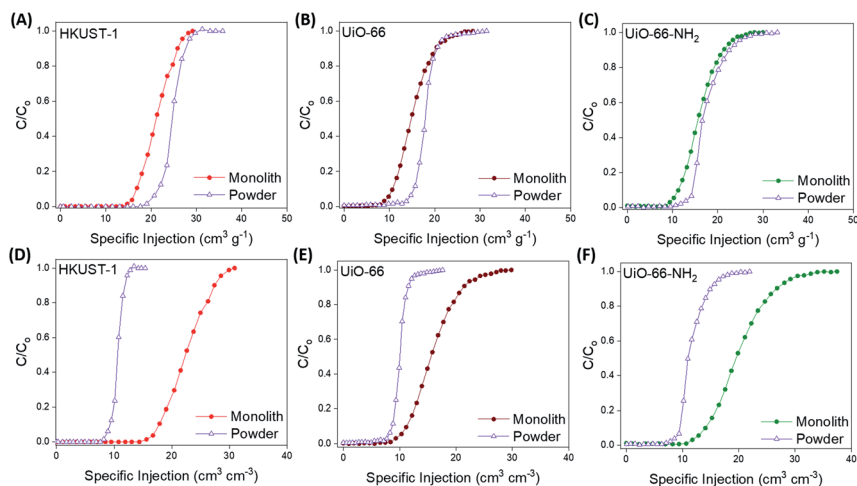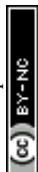

Fig. 4 Gravimetric (A–C) and volumetric (D–F) CO_2 breakthrough curves for a 15/85 v/v CO_2/N_2 gas stream at 298 K for monolithic and powdered HKUST-1, UiO-66 and UiO-66-NH$_2$ materials.
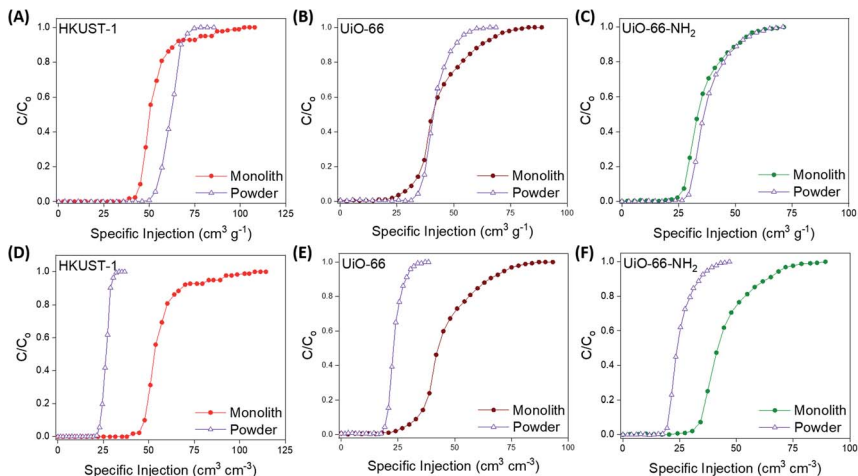
Fig. 5 Gravimetric (A–C) and volumetric (D–F) CO_2 breakthrough curves for a 50/50 v/v CO_2/CH_4 gas stream at 298 K for monolithic and powdered HKUST-1, UiO-66 and UiO-66-NH$_2$ materials.

and monolithic variants of $_{mono}$HKUST-1, $_{mono}$UiO-66 and $_{mono}$UiO-66-NH$_2$. We examined gas mixtures associated with post-combustion carbon capture (15/85 v/v CO_2/N_2, dry and 74% relative humidity) and natural gas purification (50/50 v/v CO_2/CH_4) at room temperature (Fig. 4, 5 & S33–S41†). All of the materials examined under both dry and moist conditions achieved efficient CO_2/N_2 and CO_2/CH_4 separation. N_2 and CH_4 gases eluted through the bed immediately, whereas CO_2 was retained in the adsorbent bed. For the 15/85 v/v CO_2/N_2 gas mixture, $_{mono}$HKUST-1 and the powdered variant achieved CO_2 uptake capacities of 21.3 and 24.7 cm^3 g^{-1}, respectively, under dry conditions (Table 1). The CO_2 uptake value for $_{mono}$HKUST-1 was in agreement with the IAST predicted value (Fig. S27†). Importantly, when the bulk densities of the monolithic and powdered variants of HKUST-1 were taken into account, the $_{mono}$HKUST-1 material displayed a volumetric CO_2 uptake of 22.6 cm^3 cm^{-3}, which is nearly double that of the HKUST-1 packed powder at 12.4 cm^3 cm^{-3}. Similar trends were observed for the volumetric CO_2 uptake performance of the UiO-66 (monolith = 16.0 cm^3 cm^{-3}; powder = 10.0 cm^3 cm^{-3}) and UiO-66-NH$_2$ (monolith = 20.0 cm^3 cm^{-3}; powder = 11.6 cm^3 cm^{-3}) materials for the 15/85 v/v CO_2/N_2 gas mixture (Table 1 & Fig. S34, S35†). When we exposed the materials to a humid (ca. 74% relative humidity) 15/85 v/v CO_2/N_2 gas stream, both the packed powder and monolithic MOF materials displayed a ca. 40% drop in performance compared to the dry gas mixture (Fig. S36–S38†). The drop in performance is attributed to the competitive adsorption between CO_2 and H_2O molecules.[9,32,33] Interestingly, despite this reduction in performance, the $_{mono}$MOFs exhibited nearly double the volumetric CO_2 uptake performance under humid conditions compared to the powders for each of the MOF variants studied.

When we examined the synthesized materials with the 50/50 v/v CO_2/CH_4 gas mixture, $_{mono}$HKUST-1, $_{mono}$UiO-66 and $_{mono}$UiO-66-NH$_2$ displayed exceptional volumetric CO_2 uptake values of 56.5, 44.1 and 45.2 cm^3 cm^{-3}, respectively (Table 1 & Fig. S39–S41†). The gravimetric performances of each material were in

agreement with the IAST predictions (Fig. S27–S29†). Once again, the monolithic materials significantly outperformed the packed powders in terms of the volumetric CO_2 uptake performance in the breakthrough studies, with each monolithic variant adsorbing nearly double the amount of CO_2 per cm^{-3} compared to the powdered materials. The CO_2/CH_4 separation performances of $_{mono}$HKUST-1, $_{mono}$UiO-66 and $_{mono}$UiO-66-NH$_2$ were comparable to a number of benchmark MOFs such as TIFSIX-3-Ni, NbOFFIVE-1-Ni and TIFSIX-2-Cu-i, with only materials such as Mg-MOF-74 and UTSA-16 displaying superior gravimetric CO_2 uptakes under similar conditions.[37–39,71] While many MOFs demonstrate benchmark performances for gravimetric CO_2 capture, their performances do not translate well to volumetric performance. Many studies rely on theoretical crystal densities when calculating volumetric performances, which are often not achievable during traditional MOF shaping and densification processes such as extrusion and pressing due to mechanical degradation and pore collapse.[38,50,54] Again, to the best of our knowledge, the CO_2 removal performance of $_{mono}$HKUST-1 represents the highest CO_2 removal performance achieved by any adsorbent after successful pelletisation and shaping under these conditions. Finally, we carried out recyclability tests on $_{mono}$HKUST-1, $_{mono}$UiO-66 and $_{mono}$UiO-66-NH$_2$ for the 50/50 v/v CO_2/CH_4 gas mixture (Fig. S42†). In order to examine the recyclability of the materials, we heated the adsorbents to 120 °C under a helium flow between tests. The $_{mono}$MOFs were stable under dry conditions, displaying negligible reductions in performance over five successive adsorption/desorption cycles.

Conclusions

Adsorption based gas separation processes have shown huge potential for important industrial processes such as carbon capture and gas purification. The deployment of porous adsorbents in these processes, however, has been hampered by a lack of suitable shaping processes which allow high density materials while maintaining gas sorption performance. In conclusion, we have demonstrated that $_{mono}$MOFs display superior volumetric gas separation performances compared to packed powder materials. Single-component gas adsorption isotherms suggest that all six materials examined herein are efficient at removing CO_2 from CO_2/N_2 and CO_2/CH_4 gas mixtures. However, when the bulk density of each material is evaluated to determine the volumetric performances in both gas adsorption isotherms and dynamic breakthrough studies, $_{mono}$MOFs exhibit superior CO_2 separation performances under all conditions. $_{mono}$MOFs display similar kinetics to their powdered variants, suggesting that kinetic limitations do not exist after $_{mono}$MOF synthesis. While many benchmark MOFs display exceptional gravimetric CO_2 adsorption performances, these rarely translate to volumetric CO_2 adsorption due to issues regarding MOF shaping and densification. Many reports on MOF materials rely on theoretical crystal structure densities when reporting volumetric performances, which rarely translate to experimental bulk densities upon powder processing and pelletisation. While high-density $_{mono}$MOFs have previously demonstrated benchmark performances for gas storage applications, this report represents the first demonstration of the gas separation performances of $_{mono}$MOFs. This work further illustrates the potential of this unique class of materials for a myriad of commercially relevant gas separation applications and paves the way for the development of next generation

monoMOFs with superior physical properties and enhanced gas adsorption performance.

Conflicts of interest

D. F.-J. has financial interests in the start-up company immaterial, which is seeking to commercialise metal–organic frameworks.

Acknowledgements

References

1 R. Monastersky, *Nature*, 2013, **497**, 13–14.
2 M. Hulme, *Nat. Clim. Change*, 2016, **6**, 222.
3 M. Odenberger and F. Johnsson, *Int. J. Greenhouse Gas Control*, 2010, **4**, 327–340.
4 M. E. Boot-Handford, J. C. Abanades, E. J. Anthony, M. J. Blunt, S. Brandani, N. Mac Dowell, J. R. Fernández, M.-C. Ferrari, R. Gross and J. P. Hallett, *Energy Environ. Sci.*, 2014, **7**, 130–189.
5 K. Goto, K. Yogo and T. Higashii, *Appl. Energy*, 2013, **111**, 710–720.
6 J. Rogelj, M. den Elzen, N. Hohne, T. Fransen, H. Fekete, H. Winkler, R. Schaeffer, F. Sha, K. Riahi and M. Meinshausen, *Nature*, 2016, **534**, 631–639.
7 T. Guardian, *Canada will tax carbon emissions to meet Paris climate agreement targets*, https://www.theguardian.com/world/2016/oct/03/canada-carbon-emissions-tax-paris-climate-agreement, accessed 23/01/2017, 2017.
8 A. Goeppert, H. Zhang, M. Czaun, R. B. May, G. K. S. Prakash, G. A. Olah and S. R. Narayanan, *ChemSusChem*, 2014, **7**, 1386–1397.
9 J. A. Mason, T. M. McDonald, T. H. Bae, J. E. Bachman, K. Sumida, J. J. Dutton, S. S. Kaye and J. R. Long, *J. Am. Chem. Soc.*, 2015, **137**, 4787–4803.
10 K. Sumida, D. L. Rogow, J. A. Mason, T. M. McDonald, E. D. Bloch, Z. R. Herm, T. H. Bae and J. R. Long, *Chem. Rev.*, 2012, **112**, 724–781.
11 D. M. D'Alessandro, B. Smit and J. R. Long, *Angew. Chem., Int. Ed.*, 2010, **49**, 6058–6082.
12 A. P. Hallenbeck and J. R. Kitchin, *Ind. Eng. Chem. Res.*, 2013, **52**, 10788–10794.
13 A. Sayari, A. Heydari-Gorji and Y. Yang, *J. Am. Chem. Soc.*, 2012, **134**, 13834–13842.
14 A. Sayari, Y. Belmabkhout and E. Da'na, *Langmuir*, 2012, **28**, 4241–4247.
15 A. Heydari-Gorji and A. Sayari, *Ind. Eng. Chem. Res.*, 2012, **51**, 6887–6894.
16 A. Heydari-Gorji, Y. Belmabkhout and A. Sayari, *Microporous Mesoporous Mater.*, 2011, **145**, 146–149.
17 M. Eddaoudi, J. Kim, N. Rosi, D. Vodak, J. Wachter, M. O'Keeffe and O. M. Yaghi, *Science*, 2002, **295**, 469–472.
18 L. R. MacGillivray, *Metal–organic frameworks: design and application*, John Wiley & Sons, 2010.
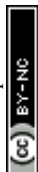
19 S. Kitagawa, R. Kitaura and S. i. Noro, *Angew. Chem., Int. Ed.*, 2004, **43**, 2334–2375.

20 P. Z. Moghadam, S. M. J. Rogge, A. Li, C.-M. Chow, J. Wieme, N. Moharrami, M. Aragones-Anglada, G. Conduit, D. A. Gomez-Gualdron, V. Van Speybroeck and D. Fairen-Jimenez, *Matter*, 2019, **1**, 219–234.

21 P. Z. Moghadam, A. Li, X.-W. Liu, R. Bueno-Perez, S.-D. Wang, S. B. Wiggin, P. A. Wood and D. Fairen-Jimenez, *Chem. Sci.*, 2020, **11**, 8373–8387.

22 B. M. Connolly, D. G. Madden, A. E. H. Wheatley and D. Fairen-Jimenez, *J. Am. Chem. Soc.*, 2020, **142**, 8541–8549.

23 K. V. Kumar, K. Preuss, M. M. Titirici and F. Rodriguez-Reinoso, *Chem. Rev.*, 2017, **117**, 1796–1825.

24 B. Li, H.-M. Wen, W. Zhou, J. Q. Xu and B. Chen, *Chem*, 2016, **1**, 557–580.

25 Q. Wang and D. Astruc, *Chem. Rev.*, 2020, **120**, 1438–1511.

26 J. P. Mehta, T. Tian, Z. Zeng, G. Divitini, B. M. Connolly, P. A. Midgley, J.-C. Tan, D. Fairen-Jimenez and A. E. H. Wheatley, *Adv. Funct. Mater.*, 2018, **28**, 1705588.

27 J. W. Osterrieth and D. Fairen-Jimenez, *Biotechnol. J.*, 2020, 2000005.

28 I. A. Lazaro and R. S. Forgan, *Coord. Chem. Rev.*, 2019, **380**, 230–259.

29 M. X. Wu and Y. W. Yang, *Adv. Mater.*, 2017, **29**, 1606134.

30 C. Orellana-Tavra, E. F. Baxter, T. Tian, T. D. Bennett, N. K. Slater, A. K. Cheetham and D. Fairen-Jimenez, *Chem. Commun.*, 2015, **51**, 13878–13881.

31 S. Mukherjee, N. Sikdar, D. O'Nolan, D. M. Franz, V. Gascon, A. Kumar, N. Kumar, H. S. Scott, D. G. Madden, P. E. Kruger, B. Space and M. J. Zaworotko, *Sci. Adv.*, 2019, **5**, eaax9171.

32 D. G. Madden, H. S. Scott, A. Kumar, K. J. Chen, R. Sanii, A. Bajpai, M. Lusi, T. Curtin, J. J. Perry and M. J. Zaworotko, *Philos. Trans. R. Soc. London, Ser. A*, 2017, **375**, 20160025.

33 A. Kumar, D. G. Madden, M. Lusi, K. J. Chen, E. A. Daniels, T. Curtin, J. J. t. Perry and M. J. Zaworotko, *Angew. Chem., Int. Ed.*, 2015, **54**, 14372–14377.

34 K. J. Chen, D. G. Madden, S. Mukherjee, T. Pham, K. A. Forrest, A. Kumar, B. Space, J. Kong, Q. Y. Zhang and M. J. Zaworotko, *Science*, 2019, **366**, 241–246.

35 A. Cadiau, K. Adil, P. M. Bhatt, Y. Belmabkhout and M. Eddaoudi, *Science*, 2016, **353**, 137–140.

36 G. Liu, V. Chernikova, Y. Liu, K. Zhang, Y. Belmabkhout, O. Shekhah, C. Zhang, S. Yi, M. Eddaoudi and W. J. Koros, *Nat. Mater.*, 2018, **17**, 283–289.

37 D. G. Madden, D. O'Nolan, K. J. Chen, C. Hua, A. Kumar, T. Pham, K. A. Forrest, B. Space, J. J. Perry, M. Khraisheh and M. J. Zaworotko, *Chem. Commun.*, 2019, **55**, 3219–3222.

38 Y. Belmabkhout, P. M. Bhatt, K. Adil, R. S. Pillai, A. Cadiau, A. Shkurenko, G. Maurin, G. Liu, W. J. Koros and M. Eddaoudi, *Nat. Energy*, 2018, **3**, 1059–1066.

39 D. Britt, H. Furukawa, B. Wang, T. G. Glover and O. M. Yaghi, *Proc. Natl. Acad. Sci. U. S. A.*, 2009, **106**, 20637.

40 A. Pichon and S. L. James, *CrystEngComm*, 2008, **10**, 1839–1847.

41 T. Friščić, D. G. Reid, I. Halasz, R. S. Stein, R. E. Dinnebier and M. J. Duer, *Angew. Chem., Int. Ed.*, 2010, **122**, 724–727.

42 K. Užarević, T. C. Wang, S.-Y. Moon, A. M. Fidelli, J. T. Hupp, O. K. Farha and T. Friščić, *Chem. Commun.*, 2016, **52**, 2133–2136.
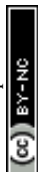
43 P. A. Julien, K. Užarević, A. D. Katsenis, S. A. Kimber, T. Wang, O. K. Farha, Y. Zhang, J. Casaban, L. S. Germann and M. Etter, *J. Am. Chem. Soc.*, 2016, **138**, 2929–2932.

44 M. Rubio-Martinez, C. Avci-Camur, A. W. Thornton, I. Imaz, D. Maspoch and M. R. Hill, *Chem. Soc. Rev.*, 2017, **46**, 3453–3480.

45 D. E. Crawford and J. Casaban, *Adv. Mater.*, 2016, **28**, 5747–5754.

46 J. Stojaković, B. S. Farris and L. R. MacGillivray, *Chem. Commun.*, 2012, **48**, 7958–7960.

47 S. L. James, C. J. Adams, C. Bolm, D. Braga, P. Collier, T. Friscic, F. Grepioni, K. D. M. Harris, G. Hyett, W. Jones, A. Krebs, J. Mack, L. Maini, A. G. Orpen, I. P. Parkin, W. C. Shearouse, J. W. Steed and D. C. Waddell, *Chem. Soc. Rev.*, 2012, **41**, 413–447.

48 R. P. Ribeiro, C. L. Antunes, A. U. Garate, A. F. Portela, M. G. Plaza, J. P. Mota and I. A. Esteves, *Microporous Mesoporous Mater.*, 2019, **275**, 111–121.

49 J. Cousin-Saint-Remi, S. Van der Perre, T. Segato, M.-P. Delplancke, S. Goderis, H. Terryn, G. Baron and J. Denayer, *ACS Appl. Mater. Interfaces*, 2019, **11**, 13694–13703.

50 A. I. Spjelkavik, S. Divekar, T. Didriksen and R. Blom, *Chem.–Eur. J.*, 2014, **20**, 8973–8978.

51 M. Tagliabue, C. Rizzo, R. Millini, P. D. Dietzel, R. Blom and S. Zanardi, *J. Porous Mater.*, 2011, **18**, 289–296.

52 Y. Hara, K. Kanamori and K. Nakanishi, *Angew. Chem., Int. Ed.*, 2019, **131**, 19223–19229.

53 M. R. Lohe, M. Rose and S. Kaskel, *Chem. Commun.*, 2009, 6056–6058.

54 S. M. Vilela, P. Salcedo-Abraira, L. Micheron, E. L. Solla, P. G. Yot and P. Horcajada, *Chem. Commun.*, 2018, **54**, 13088–13091.

55 B. Bueken, N. Van Velthoven, T. Willhammar, T. Stassin, I. Stassen, D. A. Keen, G. V. Baron, J. F. Denayer, R. Ameloot and S. Bals, *Chem. Sci.*, 2017, **8**, 3939–3948.

56 J.-W. Ye, X. Zhou, Y. Wang, R.-K. Huang, H.-L. Zhou, X.-N. Cheng, Y. Ma and J.-P. Zhang, *Sci. China Mater.*, 2018, **61**, 424–428.

57 B. M. Connolly, M. Aragones-Anglada, J. Gandara-Loe, N. A. Danaf, D. C. Lamb, J. P. Mehta, D. Vulpe, S. Wuttke, J. Silvestre-Albero, P. Z. Moghadam, A. E. H. Wheatley and D. Fairen-Jimenez, *Nat. Commun.*, 2019, **10**, 2345.

58 T. Tian, Z. Zeng, D. Vulpe, M. E. Casco, G. Divitini, P. A. Midgley, J. Silvestre-Albero, J. C. Tan, P. Z. Moghadam and D. Fairen-Jimenez, *Nat. Mater.*, 2018, **17**, 174–179.

59 J. P. Mehta, T. Tian, Z. Zeng, G. Divitini, B. M. Connolly, P. A. Midgley, J.-C. Tan, D. Fairen-Jimenez and A. E. H. Wheatley, *Adv. Funct. Mater.*, 2018, **28**, 1705588.

60 T. Tian, J. Velazquez-Garcia, T. D. Bennett and D. Fairen-Jimenez, *J. Mater. Chem. A*, 2015, **3**, 2999–3005.

61 Y. Peng, V. Krungleviciute, I. Eryazici, J. T. Hupp, O. K. Farha and T. Yildirim, *J. Am. Chem. Soc.*, 2013, **135**, 11887–11894.

62 F. Raganati, V. Gargiulo, P. Ammendola, M. Alfe and R. Chirone, *Chem. Eng. J.*, 2014, **239**, 75–86.

63 J. H. Cavka, S. Jakobsen, U. Olsbye, N. Guillou, C. Lamberti, S. Bordiga and K. P. Lillerud, *J. Am. Chem. Soc.*, 2008, **130**, 13850–13851.

64 M. Kandiah, M. H. Nilsen, S. Usseglio, S. Jakobsen, U. Olsbye, M. Tilset, C. Larabi, E. A. Quadrelli, F. Bonino and K. P. Lillerud, *Chem. Mater.*, 2010, **22**, 6632–6640.

65 J. Osterrieth, J. Rampersad, D. G. Madden, N. Rampal, L. Skoric, B. Connolly, *et al.*, *ChemRxiv*, 2021, DOI: 10.26434/chemrxiv.14291644.v2.

66 A. L. Myers and J. M. Prausnitz, *AIChE J.*, 1965, **11**, 121–127.

67 Y. Peng, V. Krungleviciute, I. Eryazici, J. T. Hupp, O. K. Farha and T. Yildirim, *J. Am. Chem. Soc.*, 2013, **135**(32), 11887–11894.

68 J. Dhainaut, C. Avci-Camur, J. Troyano, A. Legrand, J. Canivet, I. Imaz, D. Maspoch, H. Reinsch and D. Farrusseng, *CrystEngComm*, 2017, **19**, 4211–4218.

69 G. E. Cmarik, M. Kim, S. M. Cohen and K. S. Walton, *Langmuir*, 2012, **28**, 15606–15613.

70 D. Siderius, V. Shen, R. Johnson III and R. van Zee, https://adsorbents.nist.gov/, accessed, 2018, 3.

71 S. Xiang, Y. He, Z. Zhang, H. Wu, W. Zhou, R. Krishna and B. Chen, *Nat. Commun.*, 2012, **3**, 954.